communications biology

A Nature Portfolio journal

Article

https://doi.org/10.1038/s42003-025-08441-w

Exo-miR-1911-5p regulates ferroptosis to promote macrophages M2 polarization-mediated gastric cancer cisplatin resistance via MYB/AKR1B10/ACC

Zihao Kong[1,2,5], Min Zhang[3,5], Hui Yuan[4,5], Jiahao Liu[1,5], Huaiming Sang[1], Ping Zhao[1], Miao Xu[1], Chuanlong Zhu[4] ✉ & Guoxin Zhang[1] ✉

Tumor-associated macrophages (TAMs) have been implicated in fostering various hallmarks of cancer progression in gastric cancer (GC). However, the intricate molecular mechanisms underlying TAM-induced chemoresistance remain incompletely understood. Exosomes emerge as key players, mediating TAM-induced resistance to cisplatin (DDP) by regulating ferroptosis. Our investigation reveals that *exo-miR-1911-5p*, delivered to GC cells from TAMs, significantly contributes to cisplatin resistance. Specifically, direct modulation of MYB by *MiR-1911-5p* leads to decreased expression of AKR1B10, a crucial factor in preventing ferroptosis. Further exploration confirms the regulation of ACC by AKR1B10. Through targeting the MYB/AKR1B10/ACC axis, exo-miR-1911-5p inhibits ferroptosis to enhances cisplatin resistance. Additionally, *exo-miR-1911-5p* promotes M2 polarization of TAMs by targeting ARHGEF3. Collectively, our findings highlight the critical role of *exo-miR-1911-5p* in mediating cisplatin resistance through modulating the cross-talk between TAMs and GC. Targeting *exo-miR-1911-5p* could represent a promising strategy for overcoming DDP resistance in GC.

Globally, gastric cancer (GC) accounts for more than 1 million new cases, positioning it as the fifth most common form of cancer and the fourth primary reason for cancer fatality[1]. Nevertheless, the outlook for advanced gastric cancer is discouraging due to the existence of inherent or acquired resistance to chemotherapy, resulting in a pessimistic five-year survival rate[2]. Consequently, there is an immediate need to investigate the mechanism behind chemotherapy resistance.

Currently, the tumor microenvironment (TME) has gained increased attention for its role in enabling tumor survival[3]. Previous research has suggested that it promotes tumor progression, and chemotherapy resistance[4,5]. As one of the most abundant cells in TME, tumor-associated macrophages (TAMs) tend to be M2-like, which promotes tumor malignant progression[5–7]. However, the mechanism of crosstalk between macrophages and GC remains uncertain.

Exosomes are small vesicles with a diameter of 30–150 nm that mediate intercellular communication[8]. Numerous studies have highlighted the role of exosome-mediated regulation in the effectiveness of cancer chemotherapy[9–11]. The interaction between macrophages and tumor cells through exosomes has been extensively studied in various cancers, contributing to tumor advancement[12,13]. MicroRNA (miRNA), encapsulated within exosomes, mediates various physiological and pathological processes through the transfer between different cells[14]. Current studies have proved that *miR-1911-5p* can exist in exosomes and promotes migration and invasion in lung adenocarcinoma[15]. But its involvement in the regulation of tumor microenvironment and chemotherapy resistance has not been studied.

In our study, we discovered that *miR-1911-5p* is highly expressed in TAM-exosomes and significantly induces resistance to cisplatin in GC. More importantly, *exo-miR-1911-5p* specifically inhibits ferroptosis induced by cisplatin. Our study demonstrated that *exo-miR-1911-5p* strategically modulates the ACC pathway via MYB/AKR1B10 axis, playing a significant role in chemotherapy resistance. Furthermore, *exo-miR-1911-5p* was found to induce macrophage M2 polarization by modulating ARHGEF3. This research highlights that *exo-miR-1911-5p* induces cisplatin resistance by regulating the cross-talk between TAMs and GC.

[1]Department of Gastroenterology, The First Affiliated Hospital of Nanjing Medical University, Nanjing, China. [2]Department of Gastroenterology, Affiliated Drum Tower Hospital of Nanjing University Medical School, Nanjing, China. [3]Department of Gastroenterology, The Affiliated Hospital of Yangzhou University, Yangzhou, China. [4]Department of Infectious Disease, The First Affiliated Hospital of Nanjing Medical University, Nanjing, China. [5]These authors contributed equally: Zihao Kong, Min Zhang, Hui Yuan, Jiahao Liu. ✉e-mail: zhucl@njmu.edu.cn; guoxinz@njmu.edu.cn

Results

TAMs inhibit ferroptosis to induce cisplatin resistance in GC

Upon identification, TAMs exhibited high expression of M2-related markers (CD206, CD163, ARG1), along with low expression of M1-related markers (INOS) (Fig. 1A). Subsequently, non-TAMs (NTAMs) and TAMs were co-cultured with gastric cancer cells. Compared to NTAMs, TAMs significantly suppressed gastric cancer cell proliferation. However, this inhibitory effect was markedly attenuated by Fer-1/DFO (Figs. 1B–F and S2F), suggesting that TAM-mediated suppression of tumor growth is partially dependent on ferroptosis activation. The TAM group

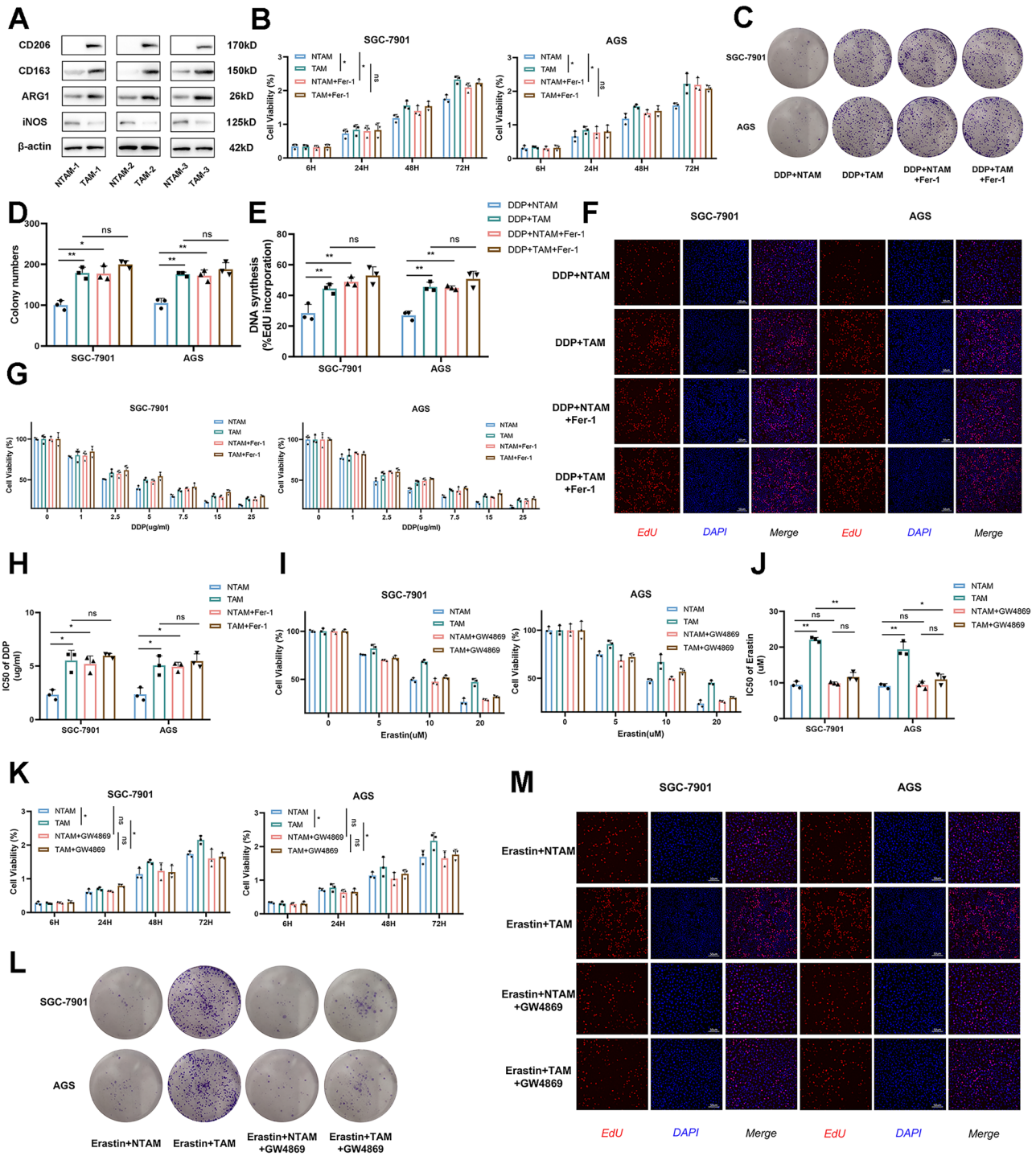

Fig. 1 | TAM inhibits ferroptosis to induce cisplatin resistance in GC. **A** Validation of macrophage polarization: Protein levels of CD206, CD163, ARG1, iNOS in TAMs from human GC tissues vs. NTAMs from normal tissues by Western blot. β-actin served as a loading control ($n = 3$); **B**–**F** Co-culture with TAMs/NTAMs in the presence or absence of Fer-1 to investigate DDP-induced malignant transformation via (**B**: CCK-8, **C**, **D**: Colony formation, **E**, **F**: EdU) ($n = 3$); **G** Relative viability of GC cells co-cultured with TAMs/NTAMs exposed to cisplatin at the indicated concentrations ($n = 3$); **H** The IC50 of GC cells treated with cisplatin ($n = 3$); **I** Relative viability of GC cells co-cultured with TAMs/NTAMs exposed to Erastin at the indicated concentrations ($n = 3$). **J** The IC50 of GC cells treated with Erastin; **K**–**M** Co-culture with TAMs/NTAMs in the presence or absence of Fer-1 to investigate Erastin-induced malignant transformation via (**K**: CCK-8, **L**: Colony formation, **M**: EdU) ($n = 3$). Representative of at least 3 experiments, data displayed as mean ± SD. $^{****}p < 0.0001$, $^{***}p < 0.001$, $^{**}p < 0.01$, $^{*}p < 0.05$.

significantly suppressed DDP-induced cell death. Interestingly, the NTAM group exhibited a notable increase in cisplatin inhibition upon the addition of Fer-1/DFO, while the inhibitory effect of the TAM group remained statistically unchanged (Figs. 1G, H and S2D, E). While the TAM group significantly suppressed DDP-induced cell death, the NTAM group exhibited enhanced cisplatin inhibition upon Fer-1/DFO treatment without statistical changes in the TAM group (Figs. 1G, H and S2D, E). Fer-1 rescued cell death, whereas autophagy inhibitors did not (Fig. S2A–C), confirming ferroptosis as the predominant mechanism. When exposed to erastin and RSL3, the TAM group effectively suppressed cell death and proliferation (Figs. 1I–M and S1A–G). However, the inhibition of ferroptosis by TAMs was abolished upon the addition of the exosome inhibitor GW4869 (Figs. 1I–M and S1A–G). Exosomes derived from TAMs/NTAMs were characterized, with size distribution analyzed via NTA, morphology assessed by TEM, and marker expression validated through Western blot (Fig. S3A–F). These findings suggest that TAMs may modulate cisplatin sensitivity by impeding ferroptosis via exosomes.

High expression of *exo-miR-1911-5p* is transferred from TAMs to GC

Compared to healthy controls in TCGA, GC patients exhibited 107 differential miRNAs (log2 |fold change| > 2, FDR < 0.05) (Fig. S4A). Analysis of exosomes from THP-1 and M2-like macrophages revealed 12 differential exo-miRNAs in GSE97467 (Fig. 2A). Through the combination of predicted genes, miRNAs (*miR-1911-5p* and *miR-135b-3p*) were identified (Fig. 2B). Significantly elevated expression of *miR-1911-5p* was observed in TCGA-STAD compared to the control group (Fig. 2C). Survival analysis of GC patients undergoing chemotherapy indicated a poorer prognosis for those with increased expression of *miR-1911-5p* (Fig. 2D). Among 10 pairs of GC tissues, only the expression of *miR-1911-5p* showed significant alteration, with higher expression observed in exosomes (Fig. 2E, F). Additionally, higher expression of *miR-1911-5p* was detected in GC cell lines (MKN-45, HGC-27, SGC-7901, BGC-823, and AGS) compared to GES-1 (Fig. 2G). Furthermore, *miR-1911-5p* was found to be highly expressed in three pairs of tumor-associated macrophages (TAMs) (Fig. 2H), particularly in exosomes (Fig. 2I).

Compared to the M0 group, GC cells co-cultured with M2-like macrophages exhibited increased expression of *miR-1911-5p*. However, this expression decreased upon the addition of GW4869 (Fig. 2K). Additionally, exosomes extracted from macrophages were successfully identified (Fig. S4B–D), and PKH26-labeled exosomes from macrophages were observed to be internalized by gastric cancer cells (Fig. 2L). In summary, *exo-miR-1911-5p* is transferred from TAMs to GC, and its high expression is associated with poor prognosis in GC.

Exosomal *miR-1911-5p* enhances cisplatin resistance in GC by inhibiting ferroptosis

To investigate the role of *miR-1911-5p* in resistance to DDP, we initially conducted transfections of cells with *miR-1911-5p* mimics and inhibitors (Fig. S5A). Treatment with *miR-1911-5p* mimics resulted in enhanced resistance to DDP (Figs. 3A, B and S5B). However, there were no discernible differences in apoptosis-related proteins between the *miR-1911-5p* mimics/inhibitor groups with DDP treatment (Figs. 3C, D and S5C).

To further explore the precise mechanism by which *miR-1911-5p* modulates resistance to DDP, we subjected GC cells to treatment with specific inhibitors targeting different cell death pathways, including the pan-caspase inhibitor Z-VAD-FMK, the necroptosis inhibitor Nec-1, and the ferroptosis inhibitor Fer-1. Interestingly, Z-VAD-FMK and Nec-1 failed to attenuate the death rate induced by DDP to the same extent as *miR-1911-5p* mimics inhibition, whereas Fer-1 achieved a comparable degree of inhibition, similar to *miR-1911-5p* inhibitor (Figs. 3E and S5D).

Furthermore, the M2 group showed marked reductions in Malondialdehyde (MDA) and lipid ROS levels, alongside an elevated GSH/GSSG ratio compared to M0; GW4869 pretreatment abolished these effects (Fig. S4E–G). Compared to the control group (NC), MDA was significantly decreased in the *miR-1911-5p* mimics group (Figs. 3G and S5E). Additionally, the level of lipid reactive oxygen species was notably downregulated in the mimics group, as evidenced by decreased green fluorescence (Figs. 3F and S5F). Overexpression of *miR-1911-5p* not only elevated the GSH/GSSG ratio (Figs. 3H and S5G), but also significantly reduced intracellular Fe^{2+} levels in *miR-1911-5p* mimics-transfected cells (Fig. 3I). Moreover, under electron microscopy, overexpression of *exo-miR-1911-5p* could reverse the mitochondrial volume reduction and membrane density increase of GC cells induced by DDP, while knocking down *exo-miR-1911-5p* exacerbated this phenomenon (Fig. 3J). In summary, *exo-miR-1911-5p*, secreted by M2-like macrophages, inhibits ferroptosis characterized by lipid peroxidation and mitochondrial dysfunction.

MiR-1911-5p regulates ferroptosis via MYB/AKR1B10 signaling pathway

To elucidate the underlying mechanism of *miR-1911-5p*, we utilized several databases, including miRDB, RNA22, TargetScan, Microt4, and miRWalk to identify potential target genes of *miR-1911-5p* (Fig. 4A). Among these candidates, *MYB* exhibited statistically significant downregulation in GC cells upon *miR-1911-5p* transfection as confirmed by qRT-PCR (Fig. 4B). Moreover, a complementary binding sequence of *miR-1911-5p* within the *MYB* gene is depicted (Fig. 4C). Subsequent luciferase activity assays revealed a significant decrease in activity upon transfection with *miR-1911-5p* mimics (Fig. 4D).

Furthermore, to analyze ferroptosis-related genes regulated by *miR-1911-5p*, we employed a ferroptosis-specific PCR array and identified numerous genes influenced by *miR-1911-5p* (Fig. 4E). Among these, *GCLC* and *AKR1B10* emerged as common differential genes with statistically significant alterations induced by *miR-1911-5p* (|fold change| >1.5, $P < 0.05$). Particularly, AKR1B10 was significantly modulated by *miR-1911-5p* (Fig. 4F). Survival analysis from TCGA-STAD data revealed that low MYB expression correlated with lower disease-free survival rates, whereas high AKR1B10 expression was associated with decreased survival rates (Fig. 4G).

Previous studies have reported that MYB acts as a transcriptional factor in most of cases[16]. To validate MYB regulate AKR1B10 as transcriptional factor, JASPAR was used to predict the binding sites of MYB and AKR1B10. Chromatin immunoprecipitation validated the binding of MYB to AKR1B10 (Fig. 4H, I), and dual-luciferase reporter assays demonstrated MYB's negative regulation of AKR1B10 (Fig. 4J, K). Western blot analysis indicated decreased MYB expression and increased AKR1B10 expression in the *miR-1911-5p* mimics group (Fig. 4L, M). Collectively, our findings provide evidence that *miR-1911-5p* negatively regulates MYB, thereby exerting a positive regulatory effect on AKR1B10.

Exo-miR-1911-5p/MYB/AKR1B10 regulates ferroptosis through ACC pathway

As depicted in Fig. 5A, the induction of cell death in GC cells by DDP was hindered by *exo-miR-1911-5p*. Conversely, cell death increased with *exo-miR-1911-5p* inhibitor (exo-inh), but this elevation was alleviated upon MYB knockdown (Fig. 5A). Si-MYB significantly decreased the levels of MDA and lipid ROS, which were elevated in the exo-inh group (Fig. 5B, C). Relative to the exo-inh group, si-MYB increased the ratio of GSH/GSSG and expression of AKR1B10, and reversed the regulatory effect of exo-inh on AKR1B10 (Fig. 5D, E). These findings further that MYB could reverse the inhibition of DDP-induced ferroptosis by *exo-miR-1911-5p*.

Acetyl-CoA carboxylase (ACC) stands as a pivotal regulator within the lipid metabolism pathway governing ferroptosis[17]. Previous study has proved that AKR1B10 interacts with ACC, preventing ACC ubiquitination and proteolysis[18]. To identify subcellular localization of AKR1B10 and ACC, we found that AKR1B10 and ACC were both localized in the cytoplasm by confocal microscopy (Fig. 5F). Subsequent co-immunoprecipitation experiments confirmed the interaction between AKR1B10 and ACC (Fig. 5G, H). Moreover, the protein expression of ACC was elevated in the exo-mimics group, and si-MYB led to an increase in ACC protein levels (Fig. 5I). ACC activity significantly increased in the *exo-miR-1911-5p*

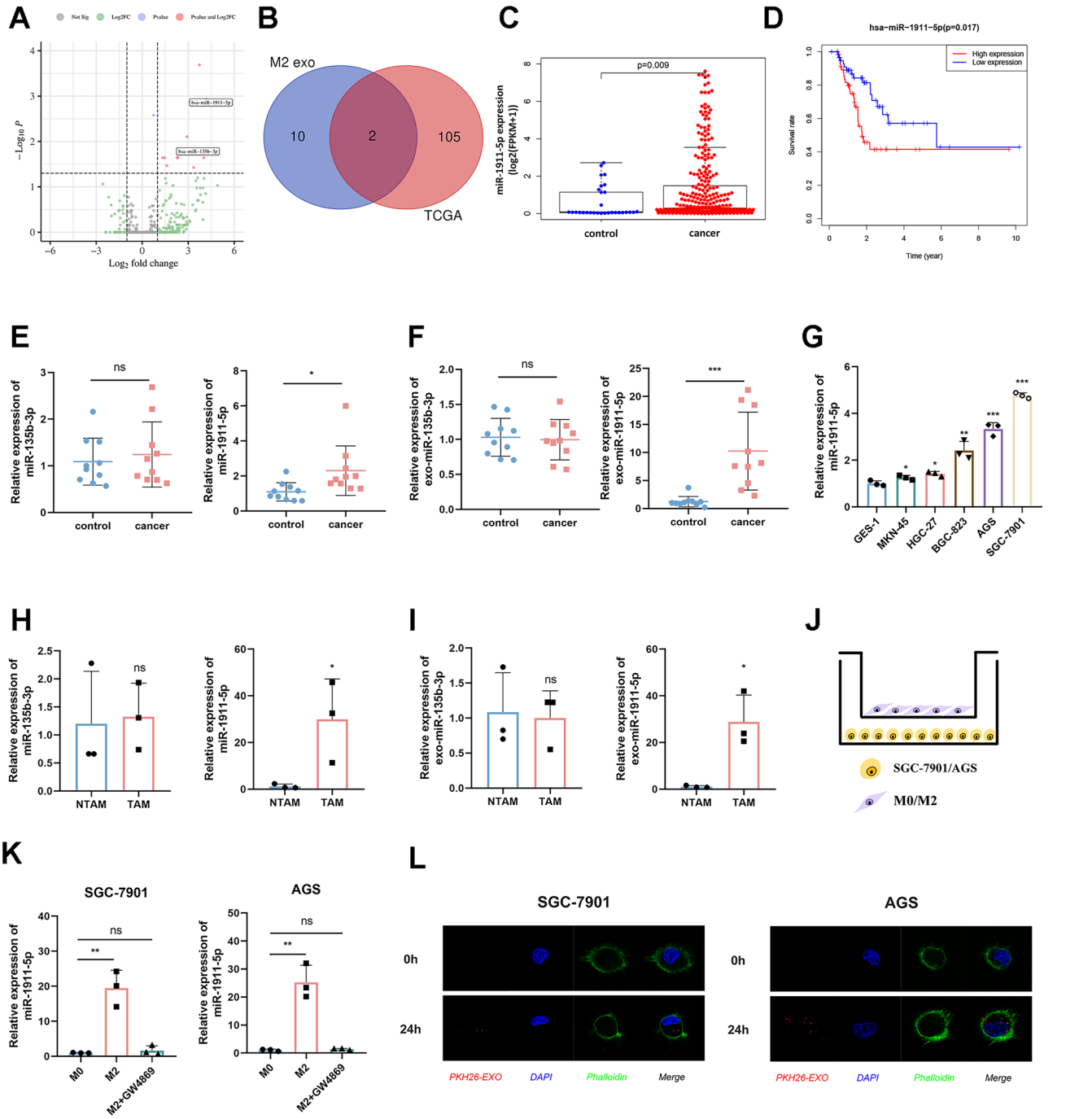

Fig. 2 | High expression of *exo-miR-1911-5p* is transferred from TAMs to GC. **A** Volcano map of different miRNA expression levels in M2-exo VS M0-exo in GSE97467; **B** Venn diagram of the intersection of differential miRNAs; **C** Expression level of *miR-1911-5p* in TCGA-STAD; **D** Survival curve of *miR-1911-5p* in patients treated with chemotherapy from TCGA-STAD; **E**, **F** qRT-PCR of *miR-1911-5p* and *miR-135b-3p* expression in GC tissues (**E**) (n = 10), exosomes from GC tissues (**F**) (n = 10); **G** Comparison of *miR-1911-5p* expression in GC cell lines and GES-1 (n = 3); **H**, **I** qRT-PCR of *miR-1911-5p* and *miR-135b-3p* expression in TAMs (**H**) (n = 3), exosomes from TAMs (**I**) (n = 3); **J** Co-culture pattern of GC cells and M2-like macrophages; **K** qRT-PCR analysis of *miR-1911-5p* expression in GC cells after co-culture and addition of GW4869 (n = 3); **L** Internalization of PKH26-labelled exosomes (red) in GC cells were observed through confocal microscopy. Representative of at least 3 experiments, data displayed as mean ± SD. $^{****}p < 0.0001$, $^{***}p < 0.001$, $^{**}p < 0.01$, $^{*}p < 0.05$.

overexpression group but was downregulated in the exo-inh group. Si-MYB could reverse the decline in ACC activity observed in the exo-inh group (Figs. 5J, K and S6A, B).

Furthermore, treatment with PF-05175157, an ACC inhibitor, resulted in increased lipid ROS (Fig. 5L) and MDA levels (Fig. 5M), along with a decreased GSH/GSSG ratio (Fig. 5N) compared to the exo-mimics group. In summary, these results demonstrate that *exo-miR-1911-5p* can regulate the ACC signaling pathway to inhibit ferroptosis.

Exo-miR-1911-5p as a therapeutic target for cisplatin resistance in vivo

To further elucidate the possible clinical significance of *exo-miR-1911-5p*, the animal experiment model diagram is presented in Fig. 6A. Compared with the PBS group, the volume and weight of the subcutaneous tumors in the M2-exo group were significantly increased, and the tumors in the *miR-1911-5p* knockdown group were significantly reduced (Figs. 6B–D and S7B–D). Western blot showed that the expression of MYB

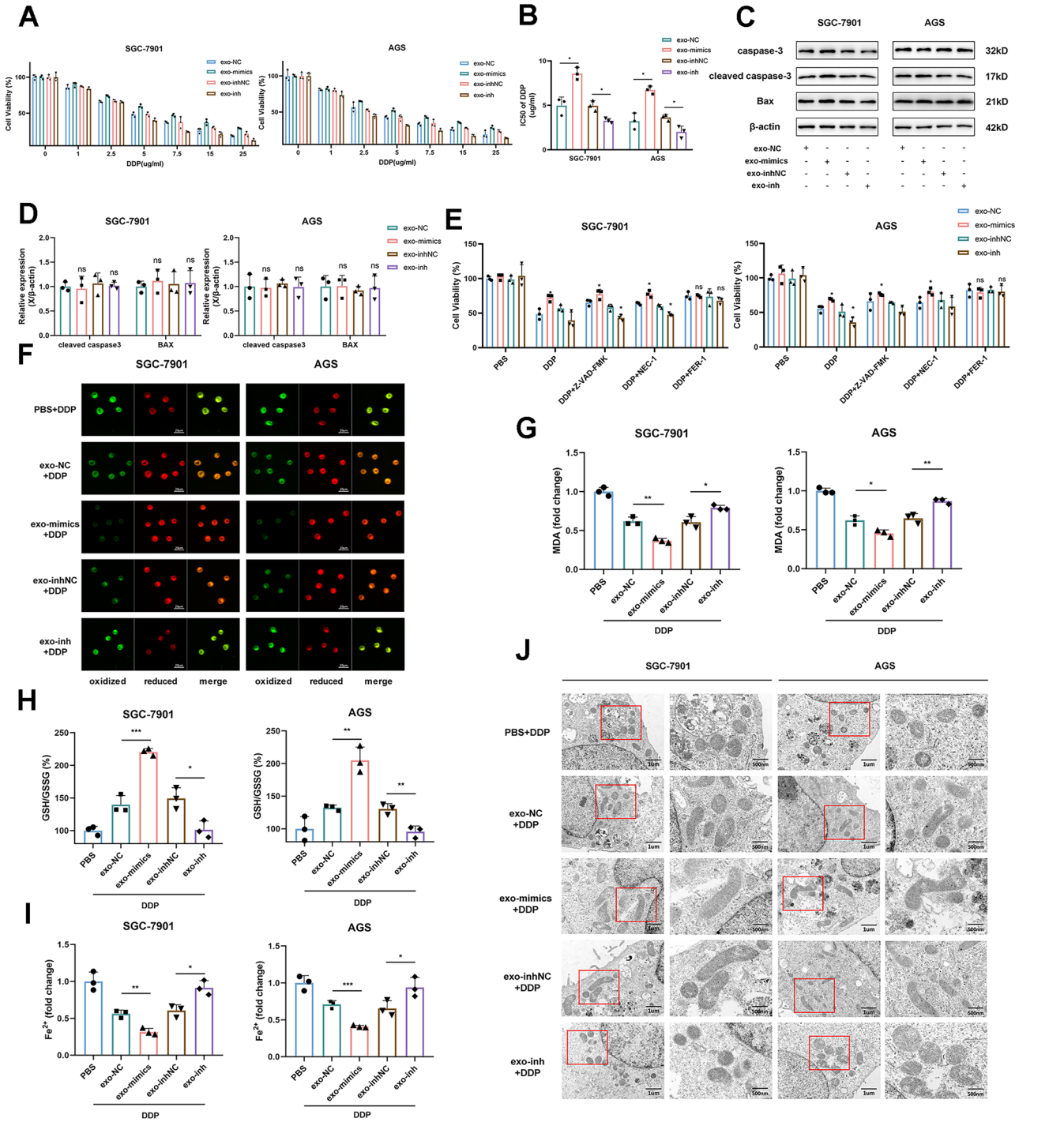

Fig. 3 | Exosomal *miR-1911-5p* enhances cisplatin resistance in GC by inhibiting ferroptosis. A Relative viability of GC cells co-cultured with exo-mimics/inhibitor exposed to cisplatin at the indicated concentrations ($n = 3$); **B** The IC50 of GC cells treated with cisplatin; **C**, **D** Expression of apoptosis-related proteins detected by Western blot ($n = 3$); **E** Cell viability of GC cells regulated by cell death inhibitors (Z-VAD-FMK, Nec-1, Fer-1) in response to DDP treatment ($n = 3$); **F–I** The phenotype of ferroptosis modulated by *exo-miR-1911-5p* (**F** Lipid peroxidation product MDA; **G** Lipid ROS; **H** GSH/GSSG ratio; **I** Fe^{2+}) ($n = 3$); **J** Electron microscopy used to view mitochondria in GC cells. Representative of at least 3 experiments, data displayed as mean ± SD. $^{****}p < 0.0001$, $^{***}p < 0.001$, $^{**}p < 0.01$, $^{*}p < 0.05$.

was upregulated and the expression of AKR1B10 and ACC was downregulated in the exo-inh group (Figs. 6E and S7E). In addition, the activity of ACC was also significantly downregulated in the exo-inh group (Figs. 6F and S7F). IHC of MYB and AKR1B10 also followed the trend of GC cell lines in vitro (Figs. 6H and S7H).

To further explore how M2-exo-*miR-1911-5p* regulates ferroptosis in vivo, we injected ferroptosis agonist IKE into three groups of nude mice (Fig. 6I). Under IKE treatment, the M2-exo group tumors were significantly larger than PBS and M2-exo-inh group (Fig. 6K, L). The results of Western blot and IHC showed that under IKE treatment, MYB was upregulated in exo-inh group compared with M2-exo group, and AKR1B10 and ACC were upregulated (Fig. 6M–O). In addition, ACC activity was downregulated in the exo-inh group (Fig. 6N). Besides, we also detected the lipid peroxidation product MDA, which revealed that the exo-inh group was elevated compared with the M2-exo group (Fig. 6P). In general, targeting *exo-miR-1911-5p* is an effective means to address GC chemotherapy resistance.

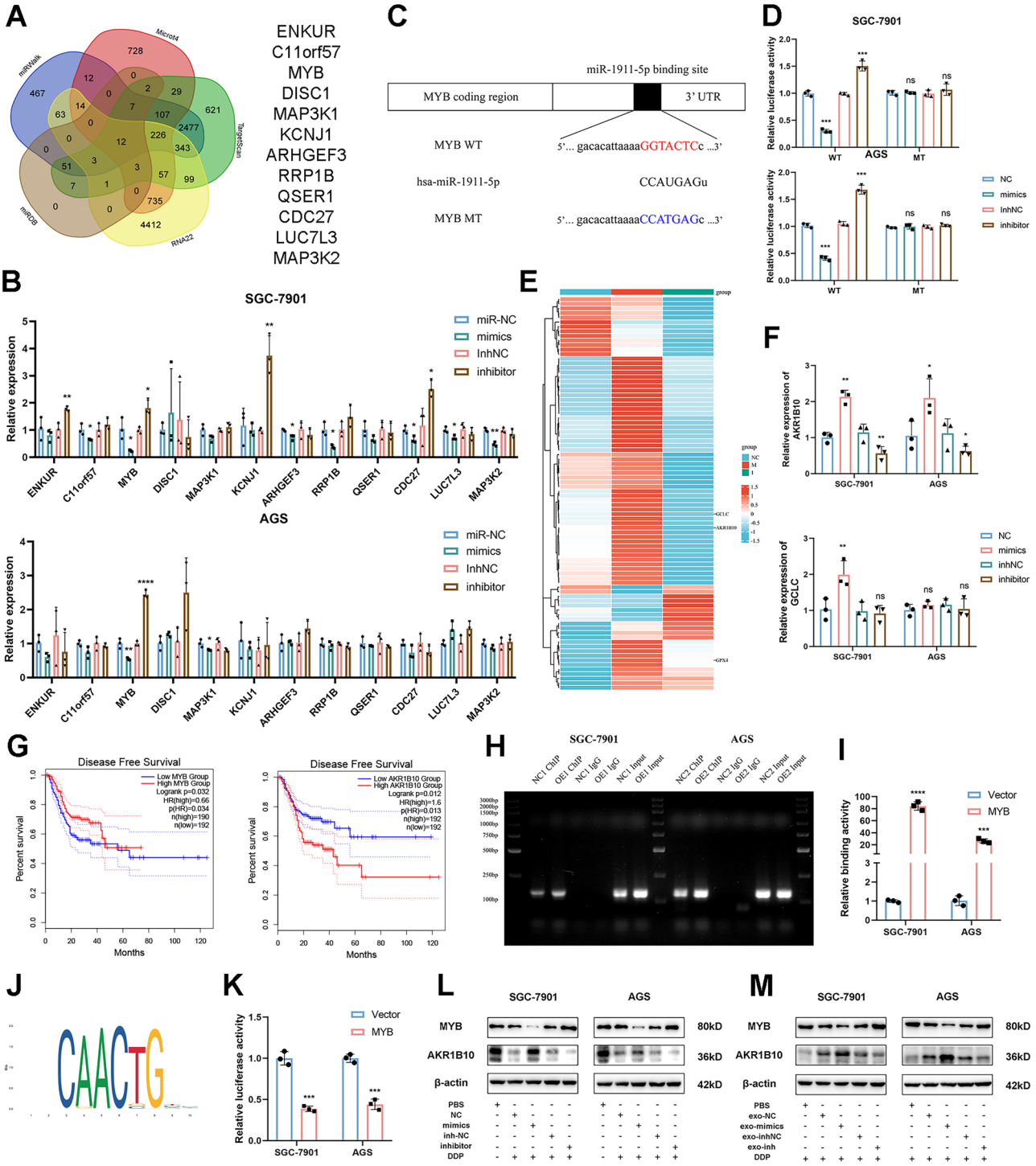

Fig. 4 | *miR-1911-5p* regulates ferroptosis via MYB/AKR1B10 signaling pathway. **A** The prediction of the *miR-1911-5p* target genes from miRDB, RNA22, TargetScan, Microt4, and miRWalk; **B** The expression of screened target genes transfected with *miR-1911-5p* ($n = 3$); **C** The mutant and putative binding site of *miR-1911-5p* with MYB; **D** Dual luciferase reporter genes to verify the regulatory relationship between *miR-1911-5p* and MYB ($n = 3$); **E** PCR array screening for ferroptosis-related genes regulated by *miR-1911-5p* ($n = 3$); **F** qRT-PCR for validation of *miR-1911-5p*-regulated ferroptosis-related genes ($n = 3$); **G** Disease-free survival curves for MYB and AKR1B10 in TCGA-STAD; **H**, **I** Chip-qpcr to verify the binding of MYB to AKR1B10; **J** Motif of MYB from JASPAR; **K** Dual luciferase reporter gene to verify that MYB negatively regulates AKR1B10 ($n = 3$); **L**, **M** The protein level of MYB and AKR1B10 after transfection with *miR-1911-5p* or *exo-miR-1911-5p*. Representative of at least 3 experiments, data displayed as mean ± SD. $^{****}p < 0.0001$, $^{***}p < 0.001$, $^{**}p < 0.01$, $^{*}p < 0.05$.

Exo-miR-1911-5p regulates ARHGEF3 to induce macrophage M2 polarization

To explore the regulatory effects of *exo-miR-1911-5p* on macrophages, we constructed a co-culture system including gastric cancer cells and macrophages (Fig. 7A). In the THP-1 cells co-cultured with GC cells overexpressing *miR-1911-5p*, the expressions of M2 polarization markers CD206, CD163, ARG-1, and IL-10 were significantly increased, while the M1-polarization markers iNOS, IL-1β were decreased, and the phenomenon disappeared after the addition of GW4869 (Fig. 7C). In addition, ELISA detection of IL-10 and IL-1β was consistent with the above results

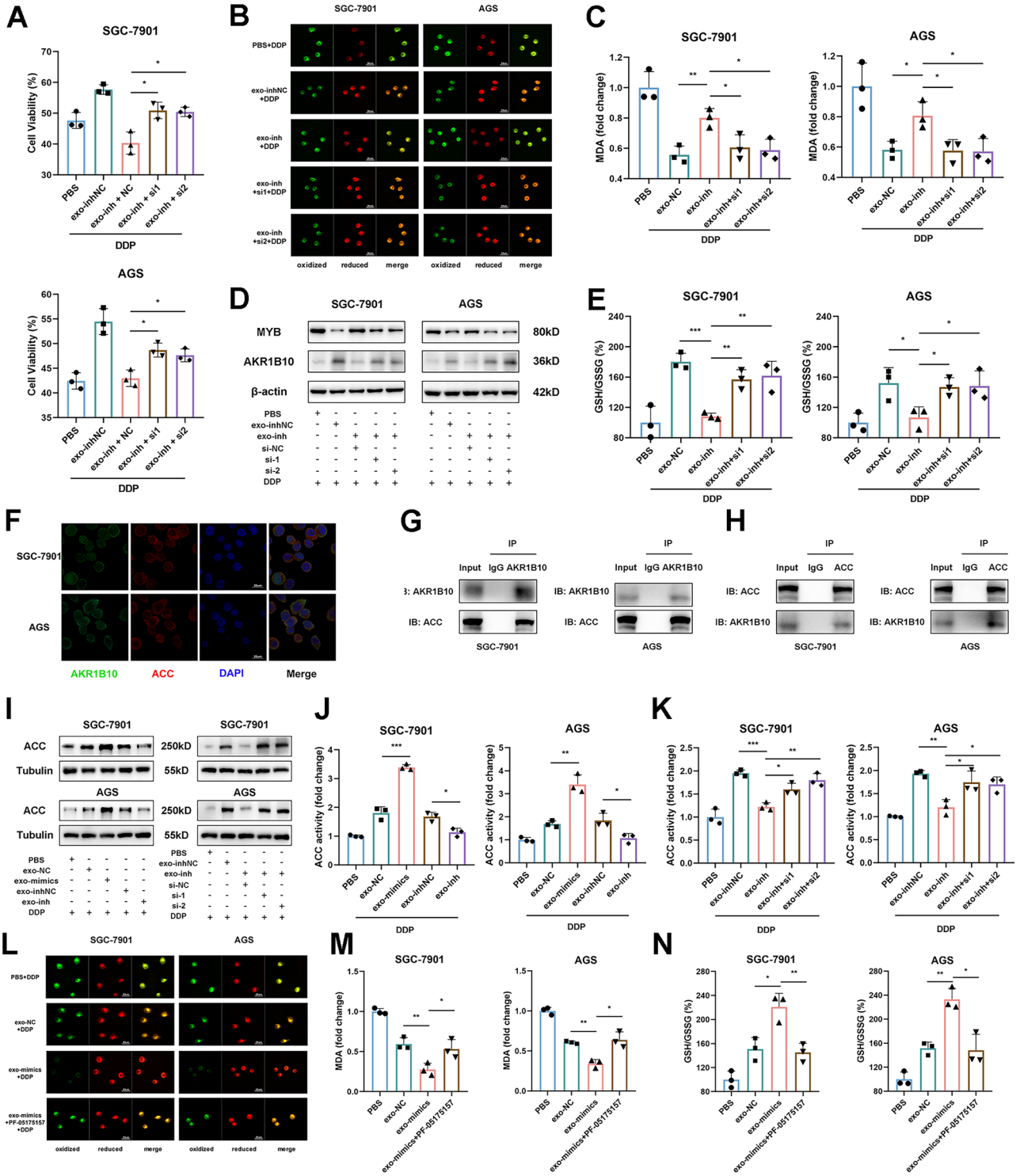

Fig. 5 | *Exo-miR-1911-5p*/MYB/AKR1B10 regulates ferroptosis through ACC pathway. **A** Cell viability after DDP stimulation detected by CCK-8 after MYB knockdown ($n = 3$); **B**, **C** Lipid peroxidation levels were detected after MYB knockdown (**B** Lipid ROS; **C** MDA) ($n = 3$); **D** Western blot was performed to detect protein levels of MYB and AKR1B10 after MYB knockdown ($n = 3$). **E** Detection of the GSH/GSSG ratio after knocking down MYB ($n = 3$); **F** Subcellular localization of AKR1B10 and ACC in GC cell lines; **G**, **H** The binding of AKR1B10 to ACC was verified by COIP experiments. **I** The expression of ACC protein were detected after exosomes addition ($n = 3$). **J** ACC activities in GC cells exposed to DDP treated with exo-mimics/inhibitor ($n = 3$); **K** ACC activities in GC cells exposed to DDP treated with exo-inhibitor/si-MYB ($n = 3$); **L**–**N** Phenotypic changes in ferroptosis after the addition of ACC inhibitors (**L** lipid ROS; **M**. MDA; **N**:GSH/GSSG) ($n = 3$). Representative of at least 3 experiments, data displayed as mean ± SD. $^{****}p < 0.0001$, $^{***}p < 0.001$, $^{**}p < 0.01$, $^{*}p < 0.05$.

(Fig. 7D). The expression levels of 12 target genes of miR-1911-5p were analyzed from the macrophage dataset GSE159112 (Fig. 7B), finding significant statistical differences in MYB, ARHGEF3, and LUC7L3. Subsequently, only ARHGEF3 in the THP-1 cell line had differences (Fig. 7C). Western blot results showed that *miR-1911-5p* mimics significantly inhibited the expression of ARHGEF3, and the expression of ARHGEF3 increased after the addition of GW4869 (Fig. 7E). We then used the dual-luciferase reporter gene to show that *miR-1911-5p* negatively regulates

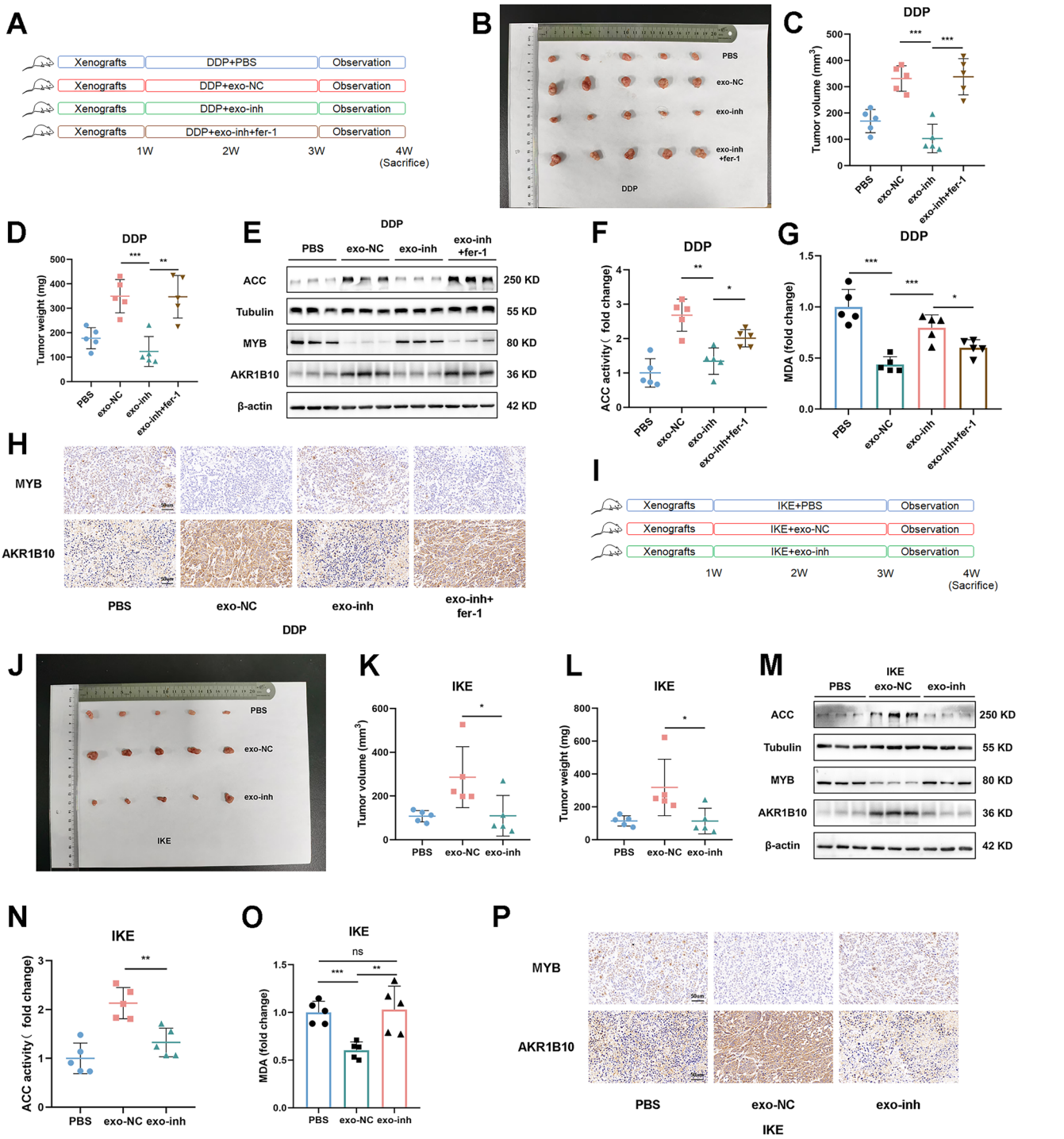

Fig. 6 | *Exo-miR-1911-5p* is a therapeutic target for cisplatin resistance in GC. **A** Groups of C57BL6 mice injected with DDP; **B** Xenograft tumors of sacrificed mice treated with cisplatin at the experimental endpoint ($n = 5$); **C** Tumor volume in each group after DDP treatment ($n = 5$); **D** Tumor weight after treatment with DDP in each group ($n = 5$); **E** Western blotting indicates expression levels of MYB, AKR1B10, and ACC ($n = 5$). **F** ACC activity in each group stimulated by DDP ($n = 5$); **G** *Exo-miR-1911-5p* suppresses MDA levels ($n = 5$); **H** IHC revealed the expression levels of MYB and AKR1B10 ($n = 5$). **I** Pattern of three groups of mice injected with IKE; **J** Xenograft tumors of sacrificed mice treated with IKE at the experimental endpoint ($n = 5$); **K, L** Tumor volume (**K**) and weight (**L**) of nude mice in each group after IKE treatment ($n = 5$); **M** The expression levels of MYB, AKR1B10, and ACC were determined by Western blot ($n = 5$); **N** ACC activity was stimulated by IKE in each group ($n = 5$); **O** IHC revealed expression levels of MYB and AKR1B10 ($n = 5$); **P***Exo-miR-1911-5p* inhibits MDA levels in the IKE group ($n = 5$). Representative of at least 3 experiments, data displayed as mean ± SD. $^{****}p < 0.0001$, $^{***}p < 0.001$, $^{**}p < 0.01$, $^{*}p < 0.05$.

ARHGEF3 (Fig. 7F). To further explore how GC-derived exosomes regulate macrophages, we extracted exosomes from GC cell lines. Electron microscopy showed that the exosomes were saucer-like (Fig. 7G), and particle size analysis (NTM) suggested that the exosomes were about 100 nm in size (Fig. 7H). When exosomes were added to M0 cells, it was found that the exosomes overexpressing *miR-1911-5p* significantly downregulated the expression of ARHGEF3 (Fig. 7I). In addition, the exosomes overexpressing *miR-1911-5p* could promote M2 polarization (Fig. 7J, K). The mechanism diagram is shown in Fig. 7L. These findings supported the results that *exo-miR-1911-5p* regulates ARHGEF3 to induce macrophage M2 polarization

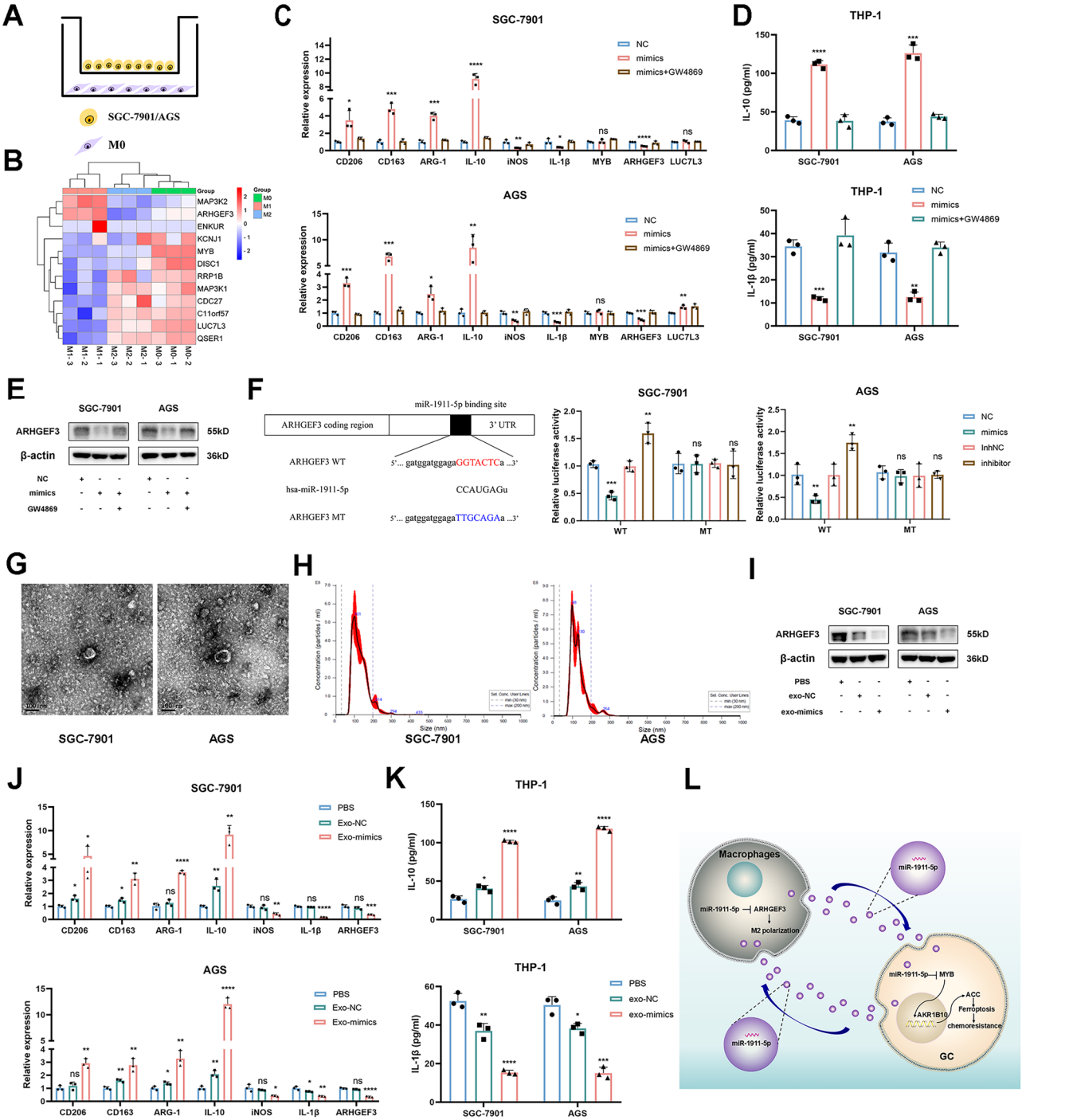

Fig. 7 | *Exo-miR-1911-5p* promotes M2 polarization in macrophages via ARHGEF3. A Co-culture pattern diagrams of M0 type macrophages and GC cell lines; **B** Heat map of *miR-1911-5p* target gene expression in M0, M1, M2-like macrophages ($n = 3$); **C** The expression of the M1/M2-like macrophages marker and *miR-1911-5p* differential target genes were analyzed using qRT-PCR ($n = 3$); **D** Detection of IL-10 and IL-1β in macrophage culture medium by Elisa ($n = 3$); **E** Western blot revealed protein expression of ARHGEF3 after transfection and treatment with GW4869 ($n = 3$); **F** Dual luciferase reporter gene reveals that *miR-1911-5p* negatively regulates ARHGEF3 ($n = 3$); **G** Morphology of exosomes under TEM; **H** The size of exosomes detected by NTA; **I** Western blot demonstrates protein expression of ARHGEF3 after exosome therapy ($n = 3$); **J** The expression of the M1/M2-like macrophahes marker and *miR-1911-5p* differential target genes after exosome stimulation analyzed by qRT-PCR ($n = 3$); **K** Detection of IL-10 and IL-1β in macrophage culture medium by Elisa ($n = 3$); **L** Mechanism diagram of this article. Representative of at least 3 experiments, data displayed as mean ± SD. $^{****}p < 0.0001$, $^{***}p < 0.001$, $^{**}p < 0.01$, $^{*}p < 0.05$.

Discussion

In the treatment for GC, cisplatin, 5-fuorouracil, paclitaxel and doxorubicin are important chemotherapeutic drugs[19]. For advanced GC, the important factor of poor prognosis is resistance to these drugs[20]. Recent research has revealed the crucial role of tumor microenvironments, specifically cancer-associated fibroblasts and tumor-associated macrophages, in cancer development[21,22]. These interactions between cells in a dynamic system are responsible for tumor progression and distant metastasis[20,23]. Our current investigation demonstrates that *exo-miR-1911-5p* enhances cisplatin resistance by facilitating the interaction between GC and TAMs, leading to the formation of an immunosuppressive microenvironment that supports tumor advancement. The intercellular interactions between

GC cells and TAMs reveals the molecular mechanism of GC cisplatin resistance.

Currently, elevated levels of *miR-1911-5p* contribute to the progression of lung adenocarcinoma[15]. However, the role of *miR-1911-5p* in GC remains unexplored. In our study, we identified that *miR-1911-5p* is upregulated in GC and correlated with the poor prognosis of GC patients. Recent studies have demonstrated that exosome-enclosed miRNAs contribute to the advancement of tumors. Increasingly evidence shows that *exo-miR-522, miR-21,* and *miR-301a-3p* were strongly associated with GC progression, recurrence, and poor prognosis[24–26]. Our study also discovered that *exo-miR-1911-5p* derived from TAMs enhances cisplatin resistance in GC. Generally speaking, *exo-miR-1911-5p* enhances cisplatin resistance in GC.

TAMs are one of the most abundant cells in the tumor microenvironment, and their interactions with GC cells have received more and more attention[22,27]. Exosomes, as small vesicles of intercellular communication, are often used to mediate material exchange between tumor microenvironment and GC cells[26], and regulate malignant behaviors[28–30]. Studies reported that TAMs-derived exosomes can enhance the DDP resistance of GC cells[25,31]. Our study proved that TAMs could transfer *exo-miR-1911-5p* to GC cells and promote DDP resistance by regulating ferroptosis via MYB/AKR1B10/ACC signaling pathway. Additionally, GC cells could transfer exosomes to TAMs for progression[32]. Our study found that GC cells transfer *exo-miR-1911-5p* and accelerate M2-like macrophages polarization. Therefore, *exo-miR-1911-5p* becomes the interaction medium between GC and TAMs.

Ferroptosis is a newly discovered form of cell death[33]. In terms of the study, cancer cells might be susceptible to ferroptosis, which are resistant to chemical treatment[34,35]. In our study, we discovered that *exo-miR-1911-5p* specifically regulates ferroptosis to promote DDP resistance in vitro and vivo. AKR1B10 has been shown to inhibits lipid peroxidation[36] and be involved in gastric cancer progression and DDP resistance[37,38]. Our experiment revealed that MYB can transcriptionally regulate AKR1B10 and that AKR1B10, in turn, can bind to ACC, thereby influencing lipid metabolism to regulate ferroptosis. Our present study demonstrates that *exo-miR-1911-5p* is an essential therapeutic target for drug resistance in gastric cancer, and the development of a specific ferroptosis therapy strategy for it could be a breakthrough in addressing chemotherapy resistance.

In this study, exosomal miR-1911-5p was identified as a critical regulator of cisplatin resistance in gastric cancer; however, the statistical power and generalizability of the findings were constrained by the limited sample size. To address this limitation, the clinical cohort will be prospectively expanded through multi-center collaborations and extended follow-up periods to enhance data robustness. Furthermore, the translational potential of these findings will be advanced through the engineering of exosomes using CRISPR-mediated modification or lipid nanoparticle (LNP) delivery systems. These strategies will be validated in patient-derived organoids and humanized PDX models to bridge mechanistic insights with clinical applications for overcoming cisplatin resistance.

Despite the limitation, this study demonstrated that elevated expression of *miR-1911-5p* predicts poor prognosis in chemotherapy GC patients, and found in vivo and in vitro models that exosome forms of *miR-1911-5p* regulate ferroptosis in gastric cancer via MYB/AKR1B10/ACC. In addition, *exo-miR-1911-5p* modulates macrophage polarization via ARHGEF3. In summary, we have proposed a signaling pathway for the regulation of drug resistance in gastric cancer and considered *exo-miR-1911-5p* as a promising therapeutic target.

Methods

Clinical specimens

The analysis of miRNA expression was conducted using R software (version 4.0.1), utilizing the TCGA and GEO databases. Patients who underwent surgery at First Affiliated Hospital of Nanjing Medical University provided a collection of 10 pairs of GC organizations and neighboring non-cancer tissues. Every participant provided an informed consent, and the research received approval from the Clinical Research Ethics Committee of The First Affiliated Hospital of Nanjing Medical University. All ethical regulations relevant to human research participants were followed.

Isolation of TAMs

The tissue is sliced into fragments with a diameter of 1 mm and then treated with 0.15 WU/mL D-Liberase (Roche) and 800 U/mL DNase I (Sigma-Aldrich) at a temperature of 37 °C for a duration of 15 min[39]. To create single-cell suspensions, the minced fresh specimens are carefully pressed through a 70-μm pore mesh and then undergo Ficoll gradient centrifugation. The cells are seed into a 6-well plate for 4 h at 37 °C in incubator.

Cell culture and transfection

The human gastric cancer cell lines (MKN-45, HGC-27, SGC-7901, BGC-823, AGS), GES-1, and THP-1 were obtained from the American Type Culture Collection (ATCC, USA). The SGC-7901 cell line, historically recognized as a standard gastric cancer model, underwent STR authentication prior to experimentation. Cells were cultured in RPMI 1640 medium (GIBCO, Brazil) with 10% FBS at 37 °C/5% CO_2. For miRNA studies, AGS/SGC-7901 cells were transfected with Lipofectamine 2000 (10 μL/well, 50 nM RNA) containing MYB siRNA, NC, miR-1911-5p mimics/inhibitors (GenePharma, China). Transfection complexes were incubated for 6 h, followed by medium replacement. Cell viability was assessed at 24 h, and samples were collected at 48 h for analysis. Table S1 lists the sequences used.

Isolation and identification of exosomes

Cells were grown in medium with exosome-free FBS and medium was collected after transfection or drug treatment. Cell culture was centrifuged at 10,000 × *g* for 20 min to obtain supernatant. Then it was transferred to centrifuge tube for centrifuging at 100,000 × *g* for 70 min. The sediments were resuspended with PBS. Exosomes were harvested after the liquid centrifuged at 100,000 × *g* for 1 h.

RNA extraction and quantitative real-time PCR (qRT-PCR)

Total RNA was extracted from clinical samples/cell lines using TRIzol (Invitrogen). Reverse transcription was performed with PrimeScript RT Kit (TaKaRa) (500 ng RNA). qRT-PCR quantified mRNA/miRNA expression, normalized to GAPDH and U6 levels. The PCR primer sequences are shown in Table S2.

Analysis of Western blot

Proteins were isolated using RIPA buffer. Cell lysates were separated by 10% SDS-PAGE, transferred onto PVDF membranes (Millipore), and detected via Bio-Rad chemiluminescence Western blotting. All antibodies were including anti-caspase 3 (#9662, Cell Signaling Technology, 1:1000), c-caspase 3 (#9661, Cell Signaling Technology, 1:1000), BAX (#2772, Cell Signaling Technology, 1:1000), MYB (sc-74512, Santa, 200 μg/ml), AKR1B10 (ab96417, Abcam, 1:1000), ACC (#3676, Cell Signaling Technology, 1:1000), tubulin (AF1216, Beyotime, 1:1000), ARHGEF3 (PA5-30608, Invitrogen, 1:2000), and β-actin (AF2811, Beyotime, 1:2000).

Dual-Luciferase reporter assay

The luciferase reporter assay was conducted according to previous documentation[40]. The measurement of luciferase activity was performed 48 h after transfection using the Dual-Luciferase Reporter System Kit (E1910, Promega, USA).

Cell viability analysis

The cell viability was detected using Cell Counting Kit-8 (MCE, Shanghai, China) to measure the cytotoxicity of DDP.

Lipid reactive oxygen species (ROS) level

Cells were treated with cultural medium containing 10 uM BODIPY ™ 581/591 C11 probe (D3861, Thermo Fisher Scientific, USA) for 30 min. The

lipid ROS level was determined by laser confocal microscope (Olympus, Tokyo, Japan).

Malondialdehyde (MDA) measurement

Proteins were extracted from the treated cells and added the MDA detection solution (S0131S, Beyotime) to the proteins. The mixture was heated at 100 °C for 15 min. After centrifugation at 12,000 × *g*, the supernatant was taken and added to the 96-well plate. The absorbance was measured at 532 nm.

GSH measurement

The collected cells were processed according to the instructions of the GSH kit (S0052, Beyotime). The measurements were performed at a wavelength of 412 nm.

Co-immunoprecipitation (Co-IP)

The working solution of 20 ug/ml antibody was mixed with the Protein and turned for 2 h at 4 °C. After that, Protein A/G immunoprecipitation magnetic beads (B23202, Biomake) were added and turned overnight at 4 °C. After magnetically separating the mixture, the supernatant was collected and placed on ice for subsequent detection. Wash three times with 200 μL washing buffer and leave to dry for 5 min. 50 μL 1 × SDS-PAGE Loading buffer was added to the magnetic bead complex, mixed evenly and heated at 95 °C for 5 min, and the supernatant was collected for SDS-PAGE detection.

Chromatin immunoprecipitation quantitative PCR (ChIP-qPCR)

The ChIP assay was carried out by the kit instructions (Thermo Fisher Scientific, USA). The JASPAR database was used to predict binding sites of transcription factors. Primers were designed and synthesized based on binding sites, and PCR amplification was performed to validate the sequences.

Enzyme-linked immunosorbent assay (ELISA)

The collected cell supernatant was added to the ELISA plate for incubation, washing and color development according to the instructions of the ELISA kit (ab185986, ab214025, Abcam). The absorbance (OD value) of each hole was measured at 450 nm wavelength.

ACC activity measurement

The ACC activity measurement was carried out according to the instructions (AKFA009M, Beijing Boxbio Science & Technology, China).

Transmission electron microscopy (TEM)

For TEM detection, cells were fixed with 2.5% glutaraldehyde overnight at 4 °C. It was washed three times by PBS. Then fixed the samples with 3% osmium tetroxide for 2 h at room temperature. It was dehydrated in ethanol, the concentration was 30%, 50%, 75%, 95%, and 100% in turn. The specimens were immersed in epoxy resin and cut into 100 nm sections using an Ultrathin microtome (RMC Boeckeler, USA). The pictures were acquired using an 80 kV transmission electron microscope (H7500 TEM) manufactured by Hitachi in Japan.

Mice model

BALB/c nude mice and C57BL6 mice (6 weeks old; female; Beijing Vital River Laboratory Animal Technology Co., Ltd, China) were randomly divided in each group with five mice. Each mouse was subcutaneously injected with GC cells (2×10^6 cells in 200 μl PBS). After 1 week of injection, DDP (2 mg/kg) or fer-1 (5 mg/kg) or IKE (40 mg/kg) were intraperitoneally injected twice a week for 2 weeks. Moreover, exosomes were injected every two days through the tail vein. After 4 weeks, the mice were sacrificed, the tumor was taken out and the samples were processed according to the subsequent experiments. Euthanasia was performed when tumor burden reached the pre-established ethical threshold of 2000 mm^3 in accordance with institutional animal welfare guidelines. All animal experiments were approved by the animal ethics committee of Nanjing Medical University and performed in compliance with the Guide for the Care and Use of Laboratory Animals. We have complied with all relevant ethical regulations for animal use. The tumour measurements and volumes permitted by the animal ethics committee were not exceeded in any of the animal experiments.

Statistics and reproducibility

For statistical analysis, GraphPad Prism 8.00 software (USA) and SPSS version 22.0 software (USA) were used. The results were presented as the average plus standard deviation of a minimum of three separate trials. To determine the statistical distinction in two or more groups, either one-way analysis of variance (ANOVA) or Student's *t* test was employed. A significance level of less than 0.05 was considered statistically significant.

Reporting summary

Further information on research design is available in the Nature Portfolio Reporting Summary linked to this article.

Data availability

All experimental datasets supporting this study can be accessed through the corresponding author following a formal data request process. Underlying numerical data for graphs are available in Supplementary Data 1. Original uncropped blots are provided in Supplementary Fig. S8.

Received: 16 June 2024; Accepted: 26 June 2025;
Published online: 15 July 2025

References

1. Sung, H. et al. Global cancer statistics 2020: GLOBOCAN estimates of incidence and mortality worldwide for 36 cancers in 185 countries. *CA Cancer J. Clin.* **71**, 209–249 (2021).
2. Van Cutsem, E., Sagaert, X., Topal, B., Haustermans, K. & Prenen, H. Gastric cancer. *Lancet* **388**, 2654–2664 (2016).
3. Blanco-Fernandez, B., Gaspar, V. M., Engel, E. & Mano, J. F. Proteinaceous hydrogels for bioengineering advanced 3D tumor models. *Adv. Sci. (Weinh.)* **8**, 2003129 (2021).
4. Binnewies, M. et al. Understanding the tumor immune microenvironment (TIME) for effective therapy. *Nat. Med.* **24**, 541–550 (2018).
5. Christofides, A. et al. The complex role of tumor-infiltrating macrophages. *Nat. Immunol.* **23**, 1148–1156 (2022).
6. Vitale, I., Manic, G., Coussens, L. M., Kroemer, G. & Galluzzi, L. Macrophages and metabolism in the tumor microenvironment. *Cell Metab.* **30**, 36–50 (2019).
7. Qian, B. Z. & Pollard, J. W. Macrophage diversity enhances tumor progression and metastasis. *Cell* **141**, 39–51 (2010).
8. Kalluri, R. & LeBleu, V. S. The biology, function, and biomedical applications of exosomes. *Science* **367**, https://doi.org/10.1126/science.aau6977 (2020).
9. Steinbichler, T. B. et al. Therapy resistance mediated by exosomes. *Mol. Cancer* **18**, 58 (2019).
10. Thakur, A., Parra, D. C., Motallebnejad, P., Brocchi, M. & Chen, H. J. Exosomes: small vesicles with big roles in cancer, vaccine development, and therapeutics. *Bioact. Mater.* **10**, 281–294 (2022).
11. Ansari, M. A. et al. Exosome-based nanomedicine for cancer treatment by targeting inflammatory pathways: current status and future perspectives. *Semin. Cancer Biol.* **86**, 678–696 (2022).
12. Guo, W., Li, Y., Pang, W. & Shen, H. Exosomes: a potential therapeutic tool targeting communications between tumor cells and macrophages. *Mol. Ther.* **28**, 1953–1964 (2020).
13. Xu, Z. et al. Role of exosomal non-coding RNAs from tumor cells and tumor-associated macrophages in the tumor microenvironment. *Mol. Ther.* **30**, 3133–3154 (2022).
14. Jeppesen, D. K. et al. Reassessment of exosome composition. *Cell* **177**, 428–445.e418 (2019).

15. Guan, B., Dai, X., Zhu, Y. & Geng, Q. M2 macrophage-derived exosomal miR-1911-5p promotes cell migration and invasion in lung adenocarcinoma by down-regulating CELF2 -activated ZBTB4 expression. *Anti-Cancer Drugs* **34**, 238–247 (2023).
16. Srivastava, S. K. et al. MYB is a novel regulator of pancreatic tumour growth and metastasis. *Br. J. Cancer* **113**, 1694–1703 (2015).
17. Lee, H. et al. Energy-stress-mediated AMPK activation inhibits ferroptosis. *Nat. Cell Biol.* **22**, 225–234 (2020).
18. Ma, J. et al. Aldo-keto reductase family 1 B10 affects fatty acid synthesis by regulating the stability of acetyl-CoA carboxylase-alpha in breast cancer cells. *J. Biol. Chem.* **283**, 3418–3423 (2008).
19. Joshi, S. S. & Badgwell, B. D. Current treatment and recent progress in gastric cancer. *CA Cancer J. Clin.* **71**, 264–279 (2021).
20. Tang, X. H. et al. Exosome-derived noncoding RNAs in gastric cancer: functions and clinical applications. *Mol. Cancer* **20**, 99 (2021).
21. Kalluri, R. The biology and function of fibroblasts in cancer. *Nat. Rev. Cancer* **16**, 582–598 (2016).
22. Gambardella, V. et al. The role of tumor-associated macrophages in gastric cancer development and their potential as a therapeutic target. *Cancer Treat. Rev.* **86**, 102015 (2020).
23. Mao, X. et al. Crosstalk between cancer-associated fibroblasts and immune cells in the tumor microenvironment: new findings and future perspectives. *Mol. Cancer* **20**, 131 (2021).
24. Zhang, H. et al. CAF secreted miR-522 suppresses ferroptosis and promotes acquired chemo-resistance in gastric cancer. *Mol. Cancer* **19**, 43 (2020).
25. Zheng, P. et al. Exosomal transfer of tumor-associated macrophage-derived miR-21 confers cisplatin resistance in gastric cancer cells. *J. Exp. Clin. Cancer Res.* **36**, 53 (2017).
26. Xia, X. et al. Hypoxic gastric cancer-derived exosomes promote progression and metastasis via MiR-301a-3p/PHD3/HIF-1α positive feedback loop. *Oncogene* **39**, 6231–6244 (2020).
27. Pathria, P., Louis, T. L. & Varner, J. A. Targeting tumor-associated macrophages in cancer. *Trends Immunol.* **40**, 310–327 (2019).
28. Miki, Y. et al. CD9-positive exosomes from cancer-associated fibroblasts stimulate the migration ability of scirrhous-type gastric cancer cells. *Br. J. Cancer* **118**, 867–877 (2018).
29. Namee, N. M. & O'Driscoll, L. Extracellular vesicles and anti-cancer drug resistance. *Biochim. Biophys. Acta Rev. Cancer* **1870**, 123–136 (2018).
30. Qu, X. et al. Loss of cancer-associated fibroblast-derived exosomal DACT3-AS1 promotes malignant transformation and ferroptosis-mediated oxaliplatin resistance in gastric cancer. *Drug Resist. Updat.* **68**, 100936 (2023).
31. Xin, L. et al. Transfer of LncRNA CRNDE in TAM-derived exosomes is linked with cisplatin resistance in gastric cancer. *EMBO Rep.* **22**, e52124 (2021).
32. Qiu, S. et al. Gastric cancer-derived exosomal miR-519a-3p promotes liver metastasis by inducing intrahepatic M2-like macrophage-mediated angiogenesis. *J. Exp. Clin. Cancer Res.* **41**, 296 (2022).
33. Stockwell, B. R. Ferroptosis turns 10: emerging mechanisms, physiological functions, and therapeutic applications. *Cell* **185**, 2401–2421 (2022).
34. Tsoi, J. et al. Multi-stage differentiation defines melanoma subtypes with differential vulnerability to drug-induced iron-dependent oxidative stress. *Cancer Cell* **33**, 890–904.e895 (2018).
35. Ouyang, S. et al. Inhibition of STAT3-ferroptosis negative regulatory axis suppresses tumor growth and alleviates chemoresistance in gastric cancer. *Redox Biol.* **52**, 102317 (2022).
36. Penning, T. M. The aldo-keto reductases (AKRs): overview. *Chem. Biol. Interact.* **234**, 236–246 (2015).
37. Matsunaga, T. et al. Aldo-keto reductase 1B10 promotes development of cisplatin resistance in gastrointestinal cancer cells through down-regulating peroxisome proliferator-activated receptor-γ-dependent mechanism. *Chem. Biol. Interact.* **256**, 142–153 (2016).
38. Morikawa, Y. et al. Acquisition of doxorubicin resistance facilitates migrating and invasive potentials of gastric cancer MKN45 cells through up-regulating aldo-keto reductase 1B10. *Chem. Biol. Interact.* **230**, 30–39 (2015).
39. Garrido-Martin, E. M. et al. M1(hot) tumor-associated macrophages boost tissue-resident memory T cells infiltration and survival in human lung cancer. *J. Immunother. Cancer* **8**, https://doi.org/10.1136/jitc-2020-000778 (2020).
40. Peng, L. et al. circCUL2 regulates gastric cancer malignant transformation and cisplatin resistance by modulating autophagy activation via miR-142-3p/ROCK2. *Mol. Cancer* **19**, 156 (2020).

Acknowledgements

Thanks for the help in the experiment of the core facilities of the First Affiliated Hospital of Nanjing Medical University. This study was supported by the National Nature Science Foundation of China (No. 81970499) and Jiangsu Province Leading Talents and Innovation Team (CXTDA2017033).

Author contributions

G.X.Z. and C.L.Z. conceived and supervised the study. H.M.S. and M.X. collected tissue samples. Z.H.K., M.Z. and H.Y. conducted experiments. Z.H.K. drafted the manuscript with H.Y. J.H.L. and P.Z. performed bioinformatics and statistical analysis. All authors have read and approved the manuscript.

Competing interests

The authors declare no competing interests.

Additional information

Supplementary information The online version contains supplementary material available at https://doi.org/10.1038/s42003-025-08441-w.

Correspondence and requests for materials should be addressed to Chuanlong Zhu or Guoxin Zhang.

Peer review information *Communications Biology* thanks the anonymous reviewers for their contribution to the peer review of this work. Primary Handling Editor: Johannes Stortz.